Evidence of local disorder in the overdoped regime of Ba(Fe_{1-x}Co_{x})_{2}As_{2}

Keeseong Park, Despina Louca, Anna Llobet, and J.-Q. Yan

Phys. Rev. B **84**, 024512 — Published 12 July 2011

DOI: 10.1103/PhysRevB.84.024512

Evidence of local disorder in the overdoped regime of $Ba(Fe_{1-x}Co_x)_2As_2$

Keeseong Park and Despina Louca
University of Virginia, Charlottesville, Virginia 22904, USA.

Anna Llobet
Lujan Neutron Scattering Center, Los Alamos National Laboratory, Los Alamos, NM 87545, USA.

J.-Q. Yan[#]
Division of Materials Science and Engineering, Ames Laboratory, Ames, IA 50011, USA.
(Dated: June 9, 2011)

The appearance of superconductivity in the antiferromagnet of $BaFe_2As_2$ with Co doping coincides with a phase transition from an orthorhombic to a tetragonal structure where coexistence of the two is observed near the phase boundary. Overdoping brings suppression of T_C near $x = 0.12$ that is not accompanied by a transition back to the orthorhombic phase. Using pulsed neutron powder diffraction, the relation of superconductivity to the atomic structure in the overdoped regime has been investigated. The suppression of superconductivity is accompanied by a structural local distortion around Co. The distortion, described as a breathing mode with alternating two or four Fe ions displaced towards Co in the ab-plane, sets in above T_C and remains in place below.

PACS numbers: 74.62.En, 61.05.F-, 74.62.Dh, 61.43.-j

The discovery of superconductivity in the Fe-based compounds, first observed in $LaFeAsO_{1-x}F_x$[1] a few years ago, has renewed the interest in the field of superconductivity. Since then, many other superconductors have been discovered within this class of materials, and significant progress has been made towards understanding their pairing mechanism and nature of their superconducting state. It is generally agreed on that spin fluctuations play an important role in the superconducting mechanism and that the nodeless $s_\pm$ is the superconducting state[2,3]. However, as more results come to surface, we find that this general argument cannot be applied uniformly in every system. For instance, magnetoelastic[4] and isotope effect[5] measurements have shown that the phonon contribution to the superconducting mechanism is not negligible. Moreover, a phonon mediated electron-electron interaction was claimed to induce a strong superconducting pairing interaction through critical d-orbital fluctuations from a five-orbital Hubbard-Holstein model calculation[6]. At the same time, the nodeless $s_\pm$ can not explain the slow suppression rate of the critical temperature (T_C) with impurity doping[7,8].

Co doping at the Fe site in the antiferromagnetic compounds of $LaFe_{1-x}Co_xAsO$[9] or $Ba(Fe_{1-x}Co_x)_2As_2$[10] induces superconductivity, in contrast to what happens in the cuprate superconductors in which doping at the Cu site would suppress superconductivity. Although doping with Co effectively introduces charge carriers[11], the excess charge appears to be mostly localized at the dopant site[12] as suggested from density functional calculations. Doping of other elements besides Co in $BaTM_2As_2$ (TM- transition metal) can give rise to similar effects where the size and relative location of the superconducting dome can be changed depending on the specific dopant[13]. However, the dopant does not carry a local magnetic moment as suggested from NMR measurements[14]. This implies that simple crystal or ligand field models cannot be applied in these systems because of their proximity to an itinerant limit in which the TM ion has charge fluctuations[15]. The extra charges from doping weaken the Fermi surface nesting condition of the parent compound, and superconductivity appears when spin density waves are suppressed[16,17]. With further electron doping, the hole pockets disappear and the absence of interband scattering is believed to suppress superconductivity[18]. A recent study comparing Co doping and the effects of applied pressure on $BaFe_2As_2$ showed that the Fe-As bond length is a key structural parameter to determining superconductivity[19]. Other parameters such as the As-Fe-As angle[20] and the As distance from the Fe layer[21] show the opposite dependence with doping compared with the effects of pressure even though increasing both doping and pressure induces superconductivity. Until recently, structural studies have been limited to investigating the average crystallographic structure. As Co goes into the structure substitutionally, it shares a site with Fe and the refined parameters between the two are constrained. Thus one may question if the substitution at the Fe site has any effect on the (Fe/Co)-As tetrahedra and whether or not it changes the (Fe/Co)-As and (Fe/Co)-(Fe/Co) coupling strength. To answer these questions, a local probe like the pair density function (PDF) analysis technique is required, because if local disorder is induced due to the presence of impurity, it would be impossible to determine from the average structure.

The crystal structure of the parent compound of one of the most intensively studied Fe-based superconductors, $BaFe_2As_2$, is well known. The tetragonal *I4/mmm* structure at room temperature changes to orthorhombic with the *Fmmm* symmetry at 140 K[22] which coincides with the appearance of antiferromagnetic (AFM) order. With chemical doping at the Ba or Fe sites, the crystal transition temperature decreases and no structural transition occurs beyond

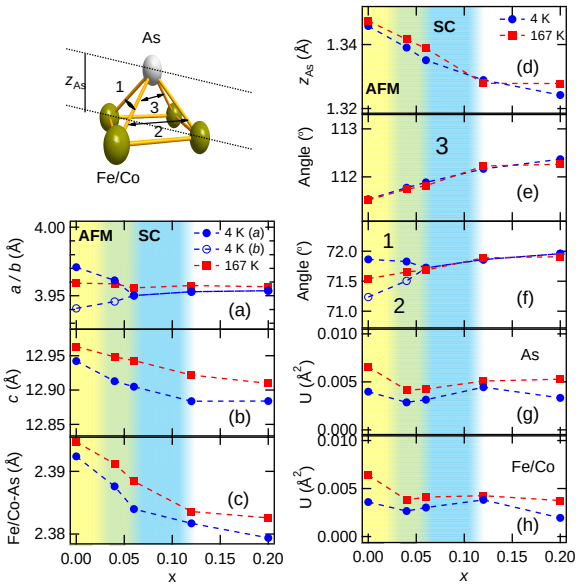

FIG. 1: The doping dependence of the lattice constants a and b (a), c (b), (Fe/Co)-As bond length (c), the anion (As) height ($z_{\rm As}$) from the Fe layer (d), the angles between (Fe/Co)-As-(Fe/Co) (e) and (f). The angles (1, 2, and 3) are defined in the diagram. The thermal parameters are also shown in (g) and (h) for As and (Fe/Co), respectively. AFM and SC regions at $T = 4$ K are shown in yellow and blue colors. Error bars are smaller than the symbols.

$x = 0.25$[23] in $Ba_{1-x}K_xFe_2As_2$ or $x = 0.063$ in $Ba(Fe_{1-x}Co_x)_2As_2$[24]. The structural transition is closely related to the appearance of superconductivity from the AFM ordered phase, but interestingly enough, no symmetry change occurs as superconductivity disappears and a normal metal state re-emerges. Here we provide evidence that shows that a local distortion develops in the normal state with Co doping in $BaFe_2As_2$. The atomic structure becomes locally distorted around the Co ions when superconductivity disappears. The local structure can be explained well by a local model involving a combination of half breathing and full breathing modes with the Fe ions displaced towards Co in the ab-plane.

The powder samples of $Ba(Fe_{1-x}Co_x)_2As_2$ with $x = 0, 0.04, 0.06, 0.12$, and 0.20 were prepared using standard solid state reaction method starting with pure Ba, Fe, As, and Co elements. The critical temperature, T_C, for each sample was determined by magnetization and the values are as follow: 10 K for $x = 0.04$, 25 K for $x = 0.06$ and no superconducting state for $x = 0.12$, and $x = 0.20$, the same as in the literature[24]. The neutron diffraction data were collected above and below T_C at the High Intensity Powder Diffractometer (HIPD) of the Lujan Neutron Scattering Center of Los Alamos National Laboratory. The average structure was determined with the Rietveld method using EXPGUI[25,26] and the results are summarized in Fig. 1. The same diffraction data were used to obtain the PDF which corresponds to the local structure. The normalized scattering intensity S(Q) was Fourier transformed to obtain the PDF[27]. The PDF method describes the probability of finding a pair of atoms at a given distance. Details can be found in Ref.[28]. The PDF method was implemented in the study of the local structure of $FeSe_{1-x}Te_x$ and showed that the Te and Se atoms do not share the same site locally, while Te hybridizes more strongly with Fe in $FeSe_{0.5}Te_{0.5}$ than in FeTe, an effect that is hardly noticeable from the average structure analysis[29].

Fig. 1 summarizes the structural parameters as a function of Co concentration. Fig. 1 (a) shows the splitting of the lattice constants a and b, and how that splitting is suppressed systematically with doping at 4 K due to the symmetry change from *Fmmm* to *I4/mmm*. As is well known, AFM is suppressed and superconductivity appears with the orthorhombic to tetragonal transition in the underdoped region. The constants a and b in the orthorhombic structure were divided by a factor of $\sqrt{2}$ to compare them with those in the tetragonal structure. The tetragonal symmetry at 167 K does not change with doping up to $x = 0.20$. The orthorhombic symmetry at 4 K changes to tetragonal at $x = 0.06$ and remains unchanged up to $x = 0.20$. The lattice constant, a, does not change at 4 K, but c decreases with doping at 4 and 167 K. The anion height ($z_{\rm As}$) in Fig. 1 (d) decreases because of the change in c. In many Fe-based superconductors, a depends on the ionic radius of the dopant but c depends on the excess charge originating from the dopant. For example, hole doping (K for Ba[23], and Mn for Fe[30]) brings about an increase in c and electron doping (Co, Ni, Rh, and Pt for Fe)[13,31] causes a decrease in c. The (Fe/Co)-As bond length is decreased by 0.5 % with $x = 0.20$. The (Fe/Co)-(Fe/Co) distance, not shown in the figure, follows the same doping dependence

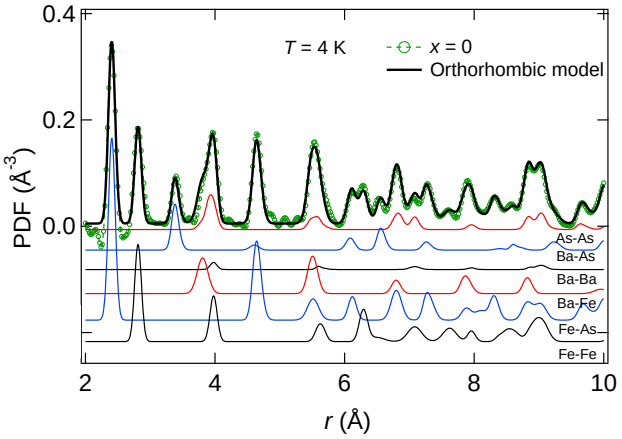

FIG. 2: The local atomic structure of $BaFe_2As_2$. The green symbol shows the experimental PDF data and the black solid line represents a model calculated from the *Fmmm* symmetry determined from the Rietveld refinement. The contributions to the PDF from each pair are also shown as solid lines with different colors.

as that of the lattice constant a. The (Fe/Co)-As-(Fe/Co) bond angles, 1, 2 and 3 in Figs. 1 (e) and (f) are not temperature dependent except at the phase transition. Angle 3 in Fig. 1 (e) expands with doping relative to the optimal angle of 109.47 [O20] and compresses the tetrahedron, $FeAs_4$, along the c-axis. Fig. 1 (g) and (h) show the thermal parameters for As and (Fe/Co), respectively. All thermal parameters at 4 K are smaller than at 167 K and remain unchanged with Co-doping. Thus the structural effects induced with Co doping are continuous and no change in the structural parameters at the phase transition from superconductivity to normal metal occurs. These results show no clear evidence as to what happens with overdoping.

In Fig. 2, the PDF corresponding to the local structure of the parent compound at 4 K is compared with a model PDF calculated using the parameters obtained from the average structure analysis with the *Fmmm* symmetry. These are: $a = 5.664$ Å, $b = 5.590$ Å, $c = 13.004$ Å, and $z = 0.3544$ of the As atom. The model PDF is calculated using $\rho(r) = 1/(4\pi N r^2) \times \sum_{\mu,\nu} \delta(r - r_\mu - r_\nu)(b_\mu b_\nu)/ < b >^2$ [28] where N is the number of atoms in the unit cell and b is the neutron scattering length of atoms, $b_{Ba} = 5.07$ fm, $b_{Fe} = 9.45$ fm, $b_{Co} = 2.47$ fm, and $b_{As} = 6.58$ fm. The partial PDF's from each pair are also shown in the figure to identify the pair contributions to the different peaks. For example, the first peak in the PDF originates from the Fe-As pairs, and the second peak originates from the Fe-Fe pairs. It can be seen that the model calculated using the orthorhombic symmetry fits the experimental data quite well. At the same time, a model using the *I/4mmm* high temperature symmetry ($a = 3.982$ Å, $c = 13.046$ Å, $z = 0.3542$ of the As atom) can fit the data at 167 K as well (not shown in the figure).

The doping dependence of the local structure is shown in Fig. 3 for $x = 0.00, 0.12$ and 0.20. The PDF is multiplied by the square of the average neutron scattering length to emphasize the effect of Co-doping. The intensity of the peaks generally decreases with increasing Co-doping because Co has a smaller neutron scattering length than Fe. At the same time, as Co doping increases, the local structure begins to show clear deviations from the average symmetry. These differences become quite pronounced by $x = 0.20$, indicated by the arrows in the figure. For instance, two new peaks emerge around the (Fe/Co)-(Fe/Co) peak at 2.8 Å, the Ba-As peak at 3.4 Å splits into two at 3.2 and 3.4 Å, and the peak split at the fourth peak around 4 Å which corresponds to the unit cell size along the a-direction is enhanced. The peak widths of the second and the third peaks of $x = 0.12$ compound are wider than those in $x = 0.20$. The wider peaks of $x = 0.12$ split into three at 2.8 Å and two peaks at 3.4 Å at $x = 0.20$. With the peak splitting, the first (Fe/Co)-As peak of $x = 0.20$ also becomes broader and its center shifts to the higher r when compared with $x = 0.12$. The changes observed in Fig. 3 cannot be explained by the changes in the scattering length. The changes in the local structure at $x = 0.20$ can be explained by a local disorder model of the Fe atoms around the Co atom, which will be described below. Here, we find that Co doping induces disorder of the (Fe/Co)-(Fe/Co) bond pair correlation and splits the peak into three parts as the system enters the normal metal state.

To understand the origin of the local disorder with Co doping, we looked into how the structure evolves with x. For comparison, in $La_{2-x}Sr_xCuO_4$, a 1:1 PDF mixture of insulating $x = 0$ and metallic $x = 0.25$ reproduces the PDF of $x = 0.15$ corresponding to the optimal doping in the system[32]. This was understood in terms of the way charges were distributed in the CuO_2 planes above and below $x = 0.15$. A similar comparison of the PDF's of a 1:1 mixture of $x = 0$ and 0.12 in $Ba(Fe_{1-x}Co_x)_2As_2$ with that of $x = 0.06$ gives a different result (Fig. 4 (c)). The PDF of $x = 0$ and $x = 0.06$, and that of $x = 0.06$ and $x = 0.12$ at 4 K are also shown in Figs. 4 (a) and (b), respectively. The first

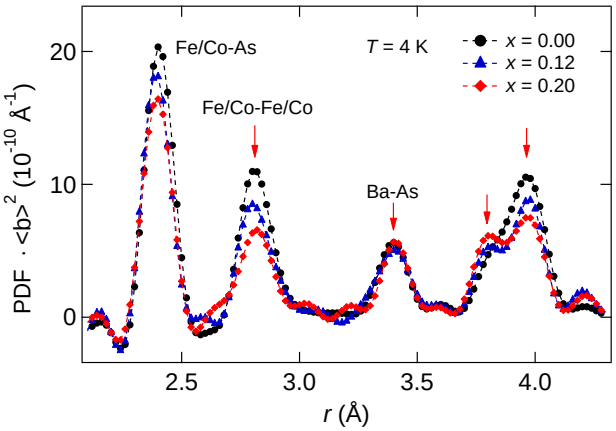

FIG. 3: The doping dependence of the first four peaks of the PDF multiplied by the square of the average scattering length for the different compositions. The first peak corresponds to (Fe/Co)-As pairs, the second to (Fe/Co)-(Fe/Co) pairs and the third to Ba-As pairs. The fourth peak at 4Å includes the contributions from four pairs, As-As, Ba-Ba, Ba-(Fe/Co), and the next nearest (Fe/Co)-(Fe/Co). The arrows indicate significant changes occurring in the local structure with doping.

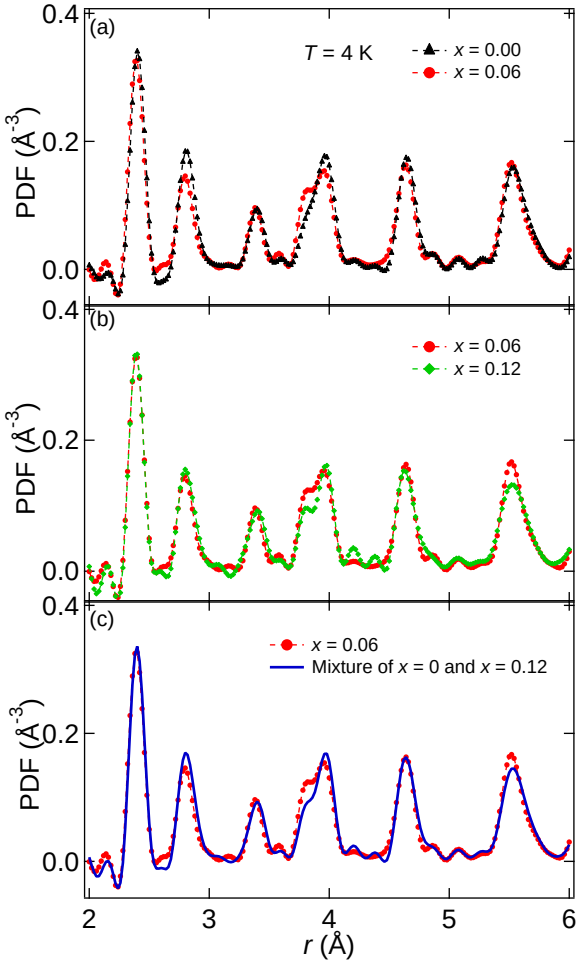

FIG. 4: The local structure of $Ba(Fe_{0.94}Co_{0.06})_2As_2$ is compared to the one obtained from a mixed phase comprised of x = 0 and 0.12. In (a), the PDF's from $x = 0.00$ and $x = 0.06$ are compared. In (b), the PDF's from $x = 0.06$ and $x = 0.12$ are compared. In (c), the PDF's from $x = 0.06$ is compared to the one obtained by combining the local structures for $x = 0.00$ and $x = 0.12$.

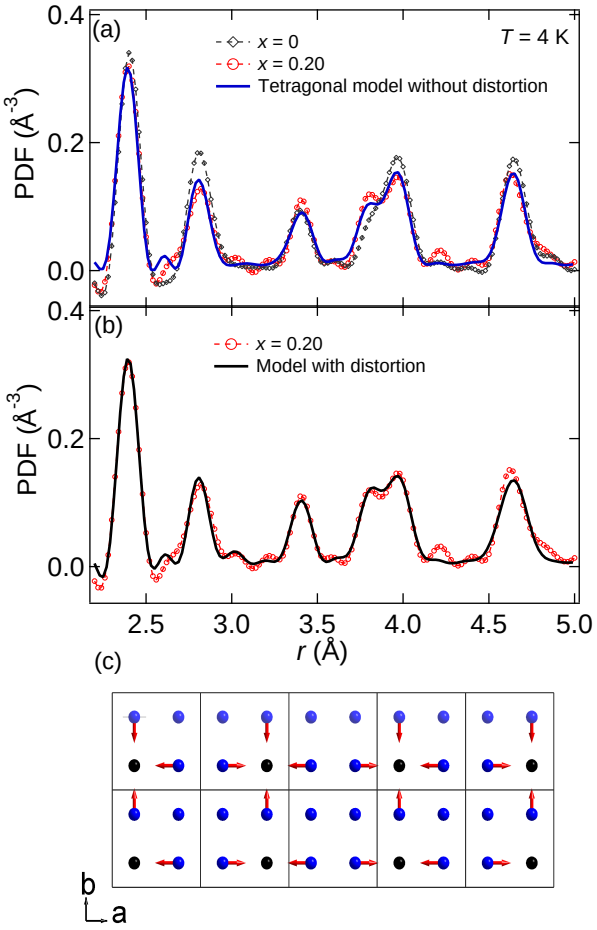

FIG. 5: The local atomic structure of $Ba(Fe_{1-x}Co_x)_2As_2$ is compared to 2 models. The red symbols correspond to the experimental PDF data at $x = 0.20$ at 4 K. Also shown is the PDF corresponding to $x = 0.0$ as the grey symbols. In (a), the blue line corresponds to a calculated PDF using the parameters from the tetragonal symmetry without any distortion. In (b), the black line corresponds to the PDF calculated using the parameters from the local distorted model shown in (c). In (c), the distorted model is shown. Only the Fe/Co atoms are shown for simplicity in the *ab*-plane. The black spheres correspond to Co atoms, and the blue ones correspond to Fe atoms. Arrows indicate the direction of displacement of the Fe atoms.

peak from (Fe/Co)-As pair at $x = 0.06$ is well described by mixing the two PDF's for $x = 0$ and 0.12 because the local bond changes monotonically up to $x = 0.12$. However, other peaks, including the (Fe/Co)-(Fe/Co) bonds, show considerable differences between the data and the mixed structure. The simple solid solution structure can explain the local structure of the optimally doped compound only up to the nearest (Fe/Co)-As bond. The metallic nature in both $x = 0$ and $x = 0.12$ in $Ba(Fe_{1-x}Co_x)_2As_2$ is different from the insulating $x = 0$ in $La_{2-x}Sr_xCuO_4$, and may make the simple mixture picture inapplicable to our system.

We fit the $x = 0.20$ data in the range between $2 - 5$ Å with a locally distorted model in order to identify the origin of the differences between the local and average structure PDFs. Fig. 5 (a) shows the experimental PDF corresponding to the local structure of $x = 0.20$ compared to a model PDF calculated using the parameters from the *I4/mmm* symmetry obtained from the average crystal structure refinement. The lattice constants were set at $a = 3.9809$ Å and $c = 13.0131$ Å, and $z = 0.3523$ for the As atom. The error propagation effect was also included using a $Q_{max} = 38$ Å^{-1} to explain the ripples at the baseline. Shown in this figure is the PDF corresponding to the parent compound to compare how the local structure of the normal state at $x = 0$ differs from the one observed with $x = 0.20$. The tetragonal symmetry describes the main peaks reasonably well but cannot reproduce the small deviations observed especially around the Fe/Co self-correlations. The crystal model is improved by introducing a local distortion around Co ions. A supercell $(5a \times 2b \times c)$ is created where $a = b = 5.6296$ Å, $c = 13.0333$ Å, and $z = 0.3527$ of the As atom (Fig. 5 (c)). This supercell size is needed to create 20 % of Co sites. It consists of 10

unit cells, which has 40 Ba atoms, 64 Fe atoms, 16 Co atoms, and 80 As atoms. Fig. 5 (c) only shows one layer of the uppermost Fe/Co sites in the $ab-$plane. In this proposed model, the Fe atoms move toward the Co atoms by 0.09(1) Å to make a full breathing mode in one row and a half breathing mode in another row. The suggested distortion by the Fe atoms improves the fit, especially in the region between 2.8 and 4 Å related to the (Fe/Co)-(Fe/Co) pairs as seen in Fig. 5 (b). The goodness of fit between the distorted model and the experimental data is given by two factors, χ^2 and R_w, and these are $\chi^2 = 0.2662$ and $R_w = 0.1754$. Without the distortion, the values are higher, where $\chi^2 = 0.3472$ and $R_w = 0.2007$. This model only describes the short range structure, up to ~ 5 Å, and cannot describe the longer-range structure fully. A more complex model needs to be implemented to describe the change at all length scales. Separately, other models have been attempted besides the one shown in this figure where the full and half breathing modes would alternate rows in different ways but yielded the same outcome. This is because the PDF model is largely insensitive to the actual real-space arrangement of distortions as long as the distances between the bond pairs yield the same length. If not, then one would expect differences in the PDF models. If we preserve the magnitude of the distortion in all directions, then the local arrangement of full and half breathing modes will not be unique. We have tested that using a supercell where the full breathing and half breathing modes alternate in rows along the a-axis and found that this model fits equally well. Thus more than one model can yield the same qualitative PDF model and would require a different probe to determine their actual arrangement.

In summary, we investigated in detail what happens to the atomic structure at the boundary between superconductivity and normal metal. The crystal structure undergoes an orthorhombic to tetragonal transition at $x = 0.06$[24] but no crystal symmetry transition is observed at the boundary between superconductivity and normal metal at 4 K. We find that local disorder develops with Co doping and by $x = 0.20$, a clear deviation of the local from the average structure is observed. To understand the change in the local structure with x, a model that includes a distortion of the Fe around Co needs to be implemented. The enhanced local disorder may be related to the suppression of superconductivity and is observed for the first time in the Fe-based superconductors. As was previously shown, superconductivity in the Fe-based superconductors is closely related to the shape of the $FeAs_4$ tetrahedra[20,21]. Moreover the exchange interactions between local moments in the Fe orbital was claimed to play a crucial role in the pairing mechanism[33]. The consideration of local disorder as suggested by this work may provide useful insights towards understanding the role of impurity in suppressing superconductivity and further aid in resolving the debate about the superconducting pairing mechanism.

#Current address: Department of Materials Science and Engineering, University of Tennessee, Knoxville, Tennessee 37996. Materials Science and Technology Division, Oak Ridge National Laboratory, Oak Ridge, Tennessee 37831.

Acknowledgments

The authors would like to acknowledge valuable discussions with R. Arita. This work is supported by the U. S. Department of Energy, Office of Basic Energy Science under contract DE-FG02-01ER45927 and DE-AC02-07CH11358. The use of HIPD at the Lujan Center at LANSCE is supported by the Division of Scientific User Facilities under contract DE-AC52-06NA25396.

[1] Y. Kamihara, T. Watanabe, M. Hirano, and H. Hosono, J. Am. Chem. Soc. **130**, 3296 (2008).
[2] D. C. Johnston, Advances in Physics **59**, 803 (2010).
[3] J. Paglione and R. L. Greene, Nat Phys **6**, 645 (2010).
[4] T. Yildirim, Phys. Rev. Lett. **102**, 037003 (2009).
[5] R. H. Liu, T. Wu, G. Wu, H. Chen, X. F. Wang, Y. L. Xie, J. J. Ying, Y. J. Yan, Q. J. Li, B. C. Shi, et al., Nature **459**, 64 (2009).
[6] H. Kontani and S. Onari, Phys. Rev. Lett. **104**, 157001 (2010).
[7] S. Onari and H. Kontani, Phys. Rev. Lett. **103**, 177001 (2009).
[8] Y. Nakajima, T. Taen, Y. Tsuchiya, T. Tamegai, H. Kitamura, and T. Murakami, Phys. Rev. B **82**, 220504 (2010).
[9] A. S. Sefat, A. Huq, M. A. McGuire, R. Jin, B. C. Sales, D. Mandrus, L. M. D. Cranswick, P. W. Stephens, and K. H. Stone, Phys. Rev. B **78**, 104505 (2008).
[10] A. S. Sefat, R. Jin, M. A. McGuire, B. C. Sales, D. J. Singh, and D. Mandrus, Phys. Rev. Lett. **101**, 117004 (2008).
[11] K. Nakamura, R. Arita, and H. Ikeda, Phys. Rev. B **83**, 144512 (2011).
[12] H. Wadati, I. Elfimov, and G. A. Sawatzky, Phys. Rev. Lett. **105**, 157004 (2010).
[13] P. C. Canfield, S. L. Bud'ko, N. Ni, J. Q. Yan, and A. Kracher, Phys. Rev. B **80**, 060501 (2009).
[14] F. Ning, K. Ahilan, T. Imai, A. S. Sefat, R. Jin, M. A. McGuire, B. C. Sales, and D. Mandrus, J. Phys. Soc. Jpn **77**, 103705 (2008).
[15] G. A. Sawatzky, I. S. Elfimov, J. van den Brink, and J. Zaanen, EPL **86**, 17006 (2009).

[16] D. J. Singh, Phys. Rev. B **78**, 094511 (2008).
[17] V. Brouet, M. Marsi, B. Mansart, A. Nicolaou, A. Taleb-Ibrahimi, P. Le Fèvre, F. Bertran, F. Rullier-Albenque, A. Forget, and D. Colson, Phys. Rev. B **80**, 165115 (2009).
[18] F. L. Ning, K. Ahilan, T. Imai, A. S. Sefat, M. A. McGuire, B. C. Sales, D. Mandrus, P. Cheng, B. Shen, and H.-H. Wen, Phys. Rev. Lett. **104**, 037001 (2010).
[19] S. Drotziger, P. Schweiss, K. Grube, T. Wolf, P. Adelmann, C. Meingast, and H. v. Löhneysen, J. Phys. Soc. Jpn **79**, 124705 (2010).
[20] C.-H. Lee, A. Iyo, H. Eisaki, H. Kito, M. T. Fernandez-Diaz, T. Ito, K. Kihou, H. Matsuhata, M. Braden, and K. Yamada, J. Phys. Soc. Jpn **77**, 083704 (2008).
[21] H. Okabe, N. Takeshita, K. Horigane, T. Muranaka, and J. Akimitsu, Phys. Rev. B **81**, 205119 (2010).
[22] M. Rotter, M. Tegel, D. Johrendt, I. Schellenberg, W. Hermes, and R. Pöttgen, Phys. Rev. B **78**, 020503 (2008).
[23] M. Rotter, M. Pangerl, M. Tegel, and D. Johrendt, Angew. Chem.,7949 **47**, 7949 (2008).
[24] S. Nandi, M. G. Kim, A. Kreyssig, R. M. Fernandes, D. K. Pratt, A. Thaler, N. Ni, S. L. Bud'ko, P. C. Canfield, J. Schmalian, et al., Phys. Rev. Lett. **104**, 057006 (2010).
[25] A. C. Larsen and R. B. von Dreele, Los Alsmos National Laboratory Report No. LAUR 86-748 (2000).
[26] B. H. Toby, J. Appl. Crystallogr. **34**, 210 (2001).
[27] B. E. Warren, H. Krutter, and O. Morningstar, Journal of the American Ceramic Society **19**, 202 (1936).
[28] T. Egami and S. J. Billinge, *Underneath the Bragg Peaks: Structural Analysis of Complex Materials* (Elsevier Science, Amsterdam, 2003).
[29] D. Louca, K. Horigane, A. Llobet, R. Arita, S. Ji, N. Katayama, S. Konbu, K. Nakamura, T.-Y. Koo, P. Tong, et al., Phys. Rev. B **81**, 134524 (2010).
[30] J. S. Kim, S. Khim, H. J. Kim, M. J. Eom, J. M. Law, R. K. Kremer, J. H. Shim, and K. H. Kim, Phys. Rev. B **82**, 024510 (2010).
[31] X. Zhu, F. Han, G. Mu, P. Cheng, J. Tang, J. Ju, K. Tanigaki, and H.-H. Wen, Phys. Rev. B **81**, 104525 (2010).
[32] E. S. Božin, G. H. Kwei, H. Takagi, and S. J. L. Billinge, Phys. Rev. Lett. **84**, 5856 (2000).
[33] R. Arita and H. Ikeda, J. Phys. Soc. Jpn **78**, 113707 (2009).